Permeation Studies on Oriented Single-Crystal Ferrierite Membranes

John E. Lewis, Jr., George R. Gavalas, and Mark E. Davis
Chemical Engineering, California Institute of Technology, Pasadena, CA 91125

Large, high-quality, single crystals of pure-silica ferrierite are synthesized, and the structure is described. Selected individual crystals (approximately 600 μm × 500 μm × 20 μm) are mounted in a membrane configuration so that only the 10-membered-ring channels (5.4 Å × 5.4 Å × 4.2 Å) or the 8-membered-ring channels (4.6 Å × 3.7 Å × 3.0 Å) are accessible for gas-molecule permeation. The first examples of transport exclusively through 8- or 10-membered-ring channel systems are reported and obtained through crystal orientation in the membrane. A series of adsorption experiments are conducted to help select suitable probe molecules and evaluate the role of adsorption in the permeation process for single-crystal membranes. Methane, n-butane, isobutane and nitrogen probe molecules are used to study intracrystalline sorption and transport effects for different crystal orientations, pressures and temperatures. Both pure-gas selectivities and mixed-gas separation factors are reported. A mixed-gas separation factor of n-butane/isobutane = 116 for the 10-membered-ring orientation of the crystal at 383 K and a transmembrane pressure difference of 1.01 × 10^5 Pa are found using this technique. In addition, molecular sieving is observed for the 8-membered-ring orientation of the crystal since methane, but not butane, transport is observed for this crystal orientation.

Introduction

Polycrystalline zeolite membranes have attracted much interest during the past decade on account of their potential for high separation selectivities and their thermal and chemical stability. This interest has been translated into remarkable developments and constant improvements in zeolite membrane preparation (Jansen and Coker, 1996). Despite these advances, a fundamental understanding of how the two fundamental measures of performance, permeance and selectivity, depend on the physical structure of the membrane has not been attained. The sieving layer of polycrystalline membranes is composed of randomly oriented individual crystallites leaving some void space between them. This void space is not necessarily connected, but any existing pathways spanning the thickness of the membrane will reduce the selectivity because they will most likely have larger diameters than the zeolitic pores. The intercrystalline contacts are quite irregular so that relating the permeance to the membrane thickness and the intrinsic crystal permeability is not a simple matter even in the absence of nonzeolitic pathways. The membrane selectivity, however, should be more closely related to the intrinsic crystal selectivity if the contribution of nonzeolitic pores and surface barriers can be neglected.

Provided the transport mechanisms remain the same for polycrystalline and single-crystal membranes, the intrinsic crystal selectivity sets an upper bound for the selectivity of multicrystalline membranes and shows to what extent this selectivity can be improved by eliminating nonzeolitic pores. Permeation measurements with single crystals then approximately define the maximum selectivity attainable with a multicrystalline membrane and, in addition, provide information about fundamental issues such as the role of crystal anisotropy, the contribution of different types of channels within a crystal, and the permeability activation energy. Here, we present a new method of preparing a single-crystal zeolite membrane and the hydrocarbon separation selectivities obtained from this system.

Correspondence concerning this article should be addressed to M. E. Davis.

The use of single-crystal membranes for gas permeation studies was inaugurated by Wernick and Osterhuber, who studied the diffusion of hydrocarbons in zeolite NaX (Wernick and Osterhuber, 1984), and by Paravar and Hayhurst, who carried out similar studies for silicalite (Paravar and Hayhurst, 1984). This work established the usefulness of single-crystal membranes as a direct method for studying diffusion in zeolites. Other techniques, such as pulse-field gradient NMR and uptake or chromatographic methods, are indirect and subject to various limitations (Kärger and Ruthven, 1992). In addition, these methods have generated diffusivity estimates differing by several orders of magnitude (Chen et al., 1994; Ruthven, 1995). Since the purpose of this work is to provide an upper bound for evaluating the properties of polycrystalline membranes, the membrane configuration and steady-state nature of the measurements is most appropriate.

Since much work on zeolite membranes involves ZSM-5 or silicalite, it is natural to pursue single-crystal measurements with the same zeolite. In fact, Shah and coworkers conducted such measurements for C_4 hydrocarbons across a single-crystal silicalite membrane (Shah et al., 1993). However, large silicalite crystals have the tendency for microtwinning along the *b*-axis (van Koningsveld, 1990) and as a result, it is very difficult to obtain true single crystals in the crystallographic sense. The complicating effects of this twinning relative to the study of the transport of hydrocarbon molecules through single-crystal silicalite membranes has been discussed (Shah and Liou, 1994). As a result of this propensity toward twinning, it is impossible to precisely define the exact free diameters of the zeolite channels and orient the crystals to study exclusively diffusion in the straight or the sinusoidal channel systems. Thus, only average diffusivities are obtained from these twinned silicalite crystal membranes (Paravar and Hayhurst, 1984), and the need for high-quality, orientable single-crystal membranes remains.

Recently, an organothermal synthesis for high-silica ferrierite was developed that yields high-quality single crystals with dimensions up to several hundred microns in size (Kuperman et al., 1993; Nadimi et al., 1995). Synthesis of this highly crystalline material has made possible detailed structure investigations (Weigel et al., 1996; Lewis et al., 1996). Based on the single-crystal structure investigation and corresponding characterization studies (Lewis et al., 1996), the defect-free nature of selected single crystals and precise dimensions of the channels were ascertained. As a result of the large crystal size, convenient morphology, and exceptional crystal quality, these ferrierite crystals are ideal candidates for the construction of oriented single-crystal membranes.

Pure-silica ferrierite has a fully condensed framework structure containing a system of intersecting channels that are circumscribed by 10 and 8 silicon atoms (Meier and Olson, 1992). The topology of the ferrierite structure is shown in Figure 1. The 10-membered-ring (MR) channels viewed along [100] are shown in Figure 1a, while the 8-MR channels viewed along [010] are shown in Figure 1b. The pores of ferrierite are not completely circular, so three slightly different pore diameters for both the 10- and 8-MR channel systems are obtained from the structure solution. Through construction of oriented single-crystal membranes and intelligent selection of probe molecule, it is possible for the first time to exploit these structural features of ferrierite and study exclusively diffusion through the 10-MR channels (5.4 Å × 5.4 Å × 4.2 Å) *or* 8-MR channels (4.6 Å × 3.7 Å × 3.0 Å).

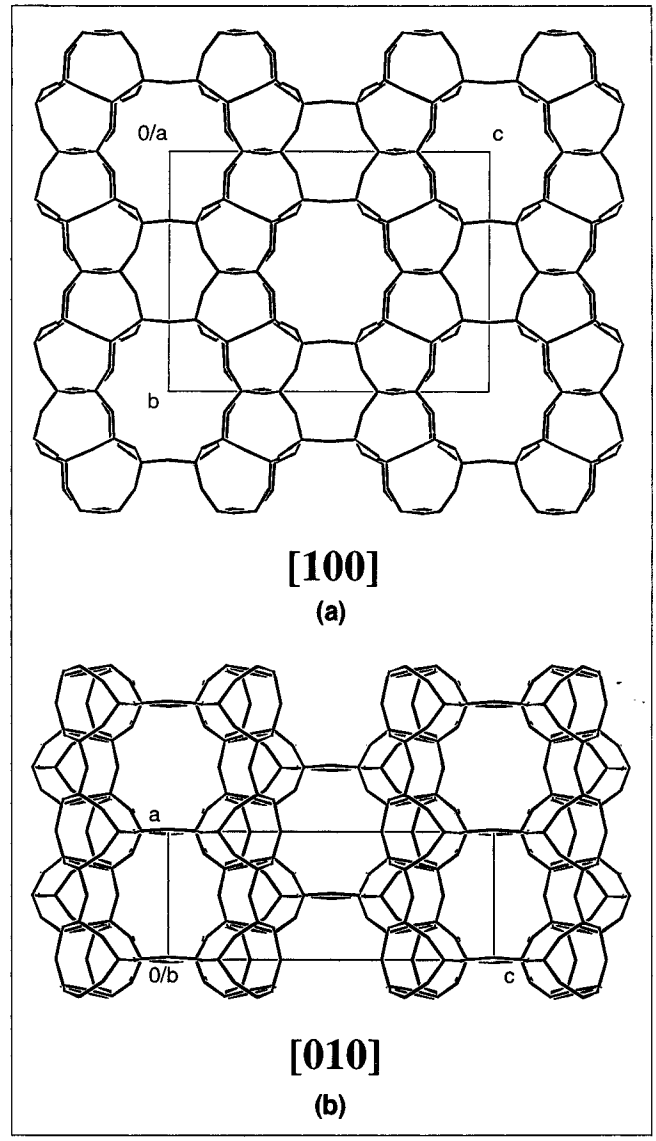

Figure 1. Ferrierite crystal structure: (a) 10 MR channels viewed down [100]; (b) 8-MR channels viewed down the [010] axis.

Unit cells denoted by rectangular boxes.

Experimental Section

Crystal synthesis and calcination

The pure-silica ferrierite crystals were prepared using an organothermal technique (Kuperman et al., 1993). The precise preparation procedures and corresponding characterization of the crystals used to construct the membranes were reported previously (Lewis et al., 1996). The general morphology and channel orientation of the crystals are shown in Figure 2. As is illustrated in Figure 2b, the 10-MR channels run parallel to the short axis of the rectangular-plate crystals, while the 8-MR channels run parallel to the longer axis of

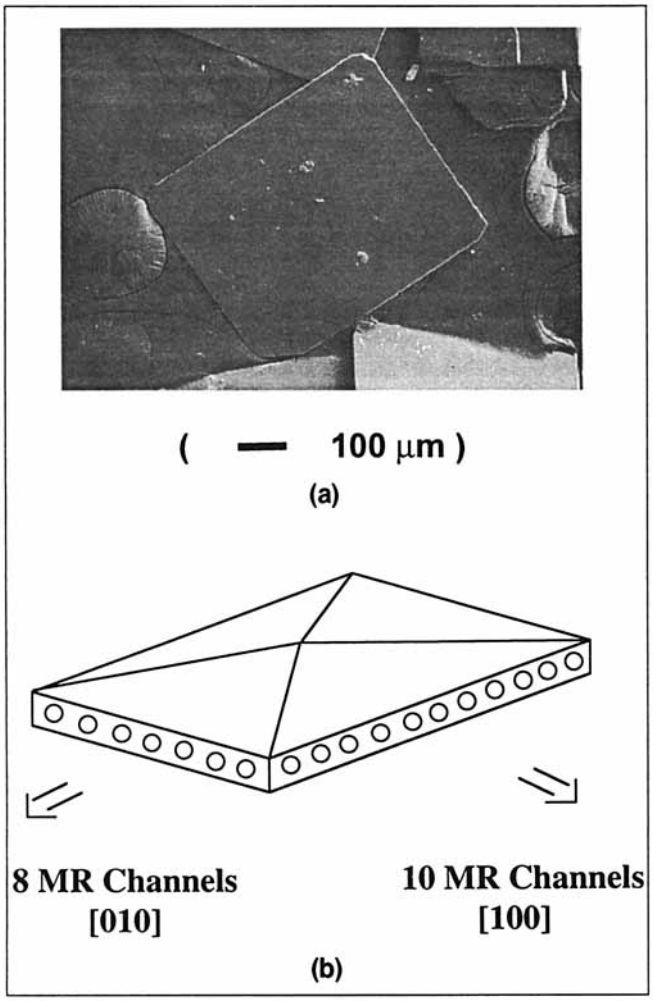

Figure 2. (a) SEM micrograph of general crystal morphology; (b) channel orientation relative to overall crystal morphology.

the rectangular plate. Thus, the only access to the micropore channel systems is via the pore mouths on the thin edges of the plate-shaped crystals. The large top and bottom sides of the plate-shaped crystals are nonporous faces composed of sheets of five MRs impervious to the probe molecules used in the adsorption and permeation experiments. A convenient feature resulting from these channel orientations relative to the crystal morphology is the fact that either the 10-MR or the 8-MR channels may be selectively chosen for study in a given single-crystal membrane.

A critical step in the preparation of the ferrierite crystals for use in membranes is the removal of the organic structure-directing agent from the as-synthesized crystals to free intracrystalline pore space for adsorption and transport. The calcination of large tetrapropylammonium-containing silicalite crystals and the effects of calcination on the crystal's inorganic framework have been studied previously (Gues et al., 1994). The development of cracks in large-crystal silicalite calcined in air has been documented (Gues and van Bekkum, 1995). As suggested from the silicalite calcination studies, initial attempts to calcine the large ferrierite crystals using conventional methods of heating in air led to severe cracking of the crystals and incomplete removal of the organic that make the crystals unsuitable for use as single-crystal membranes. The organic-free ferrierite was obtained by careful calcination of the as-synthesized material under controlled conditions to avoid damaging the single crystals. The calcination process was performed in a temperature-controlled tube furnace equipped with a valve-regulated T-shaped gas inlet connected to nitrogen and air gas cylinders. The following heating program in a controlled atmosphere yielded clear, colorless, organic-free crystals without any obvious cracking as observed by optical and scanning electron microscopy: heat in N_2 from 298 to 973 K at 1.25 K/min, hold isothermal at 973 K for 10 h in N_2, heat in air from 973 to 1,173 K at 0.83 K/min, finally hold isothermal in air at 1,173 K for 24 h. By initially heating the crystals in an inert atmosphere, the organic structure-directing agent decomposes in an endothermic manner leaving coke deposits. If the calcination is stopped at this point, the color of the crystals (originally clear) is opaque black. Switching the calcination atmosphere from nitrogen to air allows complete oxidation and removal of the decomposed organics as gases at the elevated temperatures of calcination. The separation of the decomposition and oxidation steps during calcination creates a more controlled process for removal of the organic structure-directing agents that avoids damaging the crystals.

Scanning electron microscopy

Scanning electron microscopy (SEM) images were recorded on a Camscan 2-LV scanning electron microscope using an acceleration voltage of 15 kV.

Adsorption

Nitrogen adsorption isotherms were collected on an Omnisorp 100 analyzer at 77 K with a sample weight (W) to flow rate (F) ratio of $W/F = 0.67$ g·min/cm^3 at STP (standard temperature and pressure). Hydrocarbon adsorption isotherms were recorded on a McBain-Bakr balance using a quartz spring and optical sighter to observe the degree of extension of the quartz spring. All ferrierite crystals used for adsorption (both nitrogen and hydrocarbon) were ground to micron-sized particles as determined by SEM. The reason for grinding is to remove diffusional constraints during the adsorption experiments in order to quickly obtain equilibrium adsorption isotherms. The adsorbate uptakes are reported in cm^3 of condensed liquid probe molecule per gram of ferrierite. Adsorbate kinetic diameters and their liquid densities used to calculate adsorption uptakes and their saturation pressures (P_o) for all temperatures used in the permeation experiments are reported in Table 1. These values were obtained from tables and correlations found in Breck (1974), the *CRC Handbook* (Weast et al., 1986), and Gas Processors Suppliers Association *Engineering Data Book* (GPSA, 1987).

Membrane construction

The sequence of steps used to fabricate the oriented single-crystal ferrierite membranes is shown in Figure 3. All single-crystal membranes were constructed under an optical microscope due to the delicate nature of precisely orienting and positioning the crystal. The first step is to apply a thin line of

Table 1. Physical Properties for Probe Molecules with Saturation Pressures (P_o) at Temperatures Selected for Permeation Experiments*

Physical Property and Condition	Nitrogen	Methane	*n*-Butane	Isobutane
Mol. weight [g/mol]	28.0	16.04	58.12	58.12
Boiling point [K]	77	111	272.5	261.3
Liquid density [g/cm^3]	0.808	0.424	0.601	0.549
$P_o(T = 323\ K)$ [$\times 10^{-5}$ Pa]	—	(348)	5.05	6.46
$P_o(T = 383\ K)$ [$\times 10^{-5}$ Pa]	—	(500)	17.2	23.2
$P_o(T = 398\ K)$ [$\times 10^{-5}$ Pa]	—	(600)	21.2	25.3
Kinetic diameter [Å]	3.64	3.8	4.3	5.0

*All values obtained from data and correlations given in the *CRC Handbook* (Weast et al., 1986) except for methane (in parentheses), which was estimated from data provided in the GPSA *Engineering Data Book* (GPSA, 1987). Kinetic diameters are from Breck (1974).

Torr Seal epoxy (Varian Vacuum Products) on the edge of a glass microscope cover slip (Fischer Scientific). While holding the prepared glass slip vertically under the optical microscope, a calcined ferrierite crystal is selected and carefully positioned on the thin line of epoxy using a metal probe with a very fine tip. At this point, the channel system and pore size of the single-crystal membrane is determined as either 10 or 8 MR, depending on crystal orientation. This intermediate point in the membrane construction is shown in Figure 3a. Next, the half-constructed membrane is placed in a guide constructed of glass microscope slides. A thin line of Torr Seal epoxy is placed on the edge of a second glass cover slip. Again under the microscope, the second prepared glass slip is inserted into the tracks of the guide and slowly slid up to the first glass slip and crystal. At this point, the oriented, single crystal of ferrierite is sandwiched between the two glass cover slips and embedded in epoxy in all places except for the two exposed edges (front and back) of the crystal as shown in Figure 3b. The thin-line feature in the center of the SEM micrograph is the protruding edge of the ferrierite crystal. The rough-surfaced region surrounding the crystal is the epoxy and the smooth surfaces on either side of the epoxy are the glass cover slips. The membrane is left in the guide to maintain proper positioning and alignment of the crystal and glass cover slips as the epoxy is allowed to cure at room temperature for 24 h. At this point the membrane is removed from the guide and two 15-cm-long glass tubings are attached perpendicular to either side of the membrane using epoxy, as shown in the cross-sectional view of Figure 4. These attached segments of glass tubing are used to connect the membrane to the permeation apparatus using Ultra-Torr fittings. A control experiment was also conducted by constructing the device without a crystal. No hydrocarbon flux was observed for this control membrane as detected by gas chromotography (*vide infra*), thus demonstrating the tight seal provided by the epoxy.

Permeation measurements

The experimental apparatus and sampling procedure used for measuring hydrocarbon flux through the oriented single-crystal ferrierite membranes is shown in Figure 5. The hydrocarbon flux through zeolite membranes is commonly measured either by the pressure-rise technique using sensitive pressure transducers or by the steady-state technique of flowing a feed gas from one side of the membrane and a carrier gas from the other side. Initial attempts in this study to use the pressure-rise technique failed because the cross-sectional area of the ferrierite crystal in the membrane available for permeation is too small for the flux to be measured with reasonable accuracy. Subsequently, the steady-state technique was applied, collecting the hydrocarbon permeate in a sampling loop constructed of 1/16-in. (1.6-mm) stainless-steel tubing and submerged in a liquid nitrogen bath as shown in Figure 5a. By injecting known quantities of hydrocarbons into the apparatus, it was verified that the hydrocarbon permeate

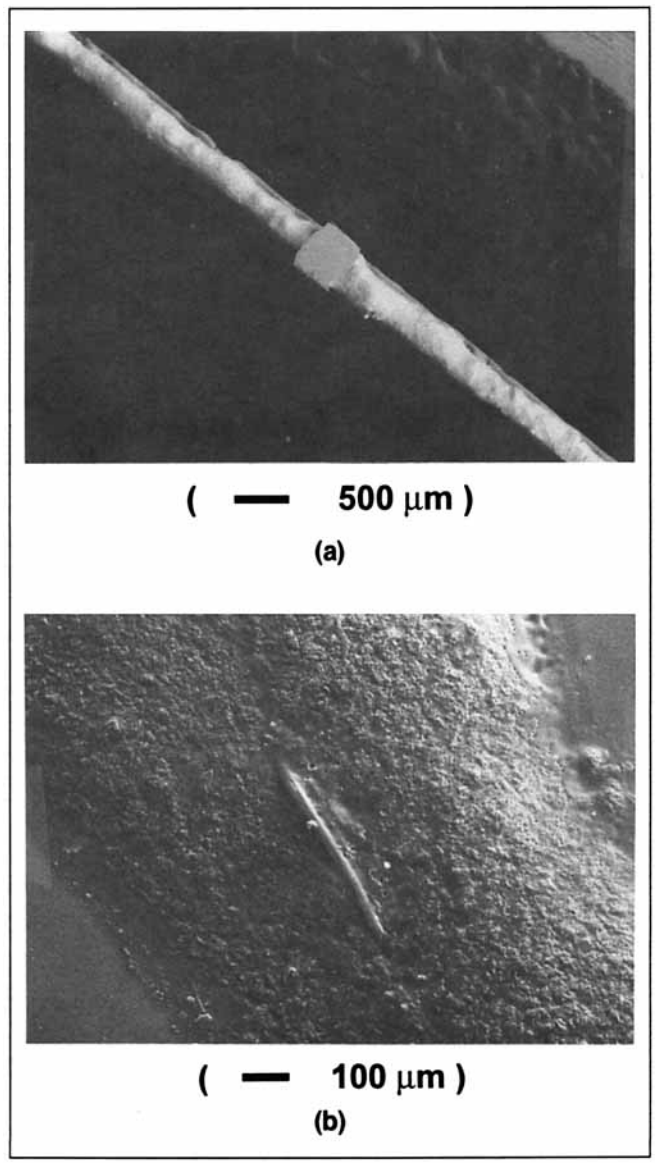

Figure 3. Sequence of steps used to fabricate the oriented single-crystal ferrierite membranes.

(a) Half-completed membrane of crystal in 8-membered-ring orientation; (b) completed membrane of protruding crystal edge embedded in epoxy and sandwiched between two glass cover slips.

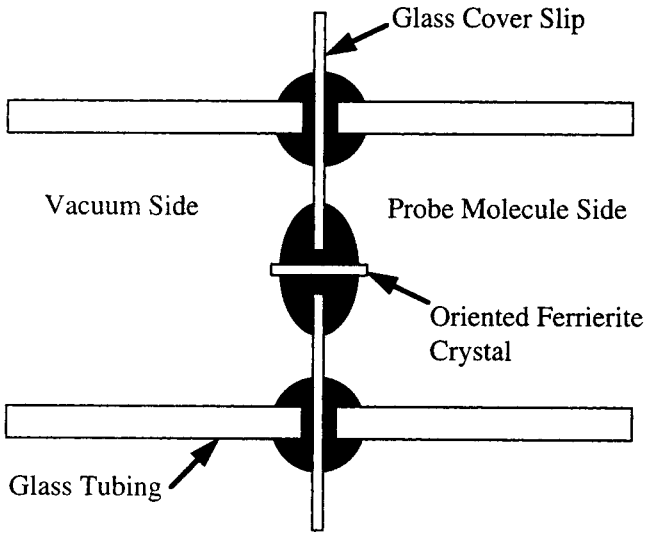

Figure 4. Attachment of glass tubing segments for incorporation of membrane into permeation measurement apparatus.

Shaded regions indicate junctions between glass tubing, glass cover slips, and crystal sealed with epoxy.

is quantitatively trapped as it passes through the chilled sampling loop. Permeate can be collected over a sufficiently long period of time (typically 15 min to 10 h) to obtain adequate sample for gas chromatographic determination. To ensure that the sampling loop did not become plugged with condensate during the sample collection period, the sample collection time was doubled to make sure the amount of collected hydrocarbon detected also doubled before finalizing the measurement conditions. This test verifies that the pressure on the permeate side of the crystal remains approximately zero and a constant membrane pressure differential, that is, driving force, is maintained throughout the permeate collection period.

After collecting permeate for a given length of time, the sample loop is isolated from the rest of the system by closing the four-way valve and removing the sample loop from the liquid nitrogen bath as shown in Figure 5b. The collected permeate is allowed to warm to room temperature and is then swept into the gas chromatograph (GC) with helium by adjusting the four- and six-way valves, as shown in Figure 5c. The amount of hydrocarbon collected during the sampling phase of the permeation experiment is measured using a Hewlett-Packard 5890 Series II GC equipped with a flame ionization detector (FID). An Alltech chromatographic column packed with 0.17% picric acid on Graphpac and GC responses were recorded on a Hewlett-Packard 3394A integrator. The gas chromatograph was calibrated using a calibration gas mixture of *n*-butane and isobutane, 1025 ppm and 985 ppm, respectively, in nitrogen from Matheson Gas Products, Inc. The FID responses for methane were quantified using sensitivity factors relative to the calibrated butane responses (Dietz, 1967). At the conclusion of a permeation experiment, the cross-sectional area of the embedded crystal available for gas flux was measured by SEM. With the amount of hydrocarbon collected, collection time, crystal cross-sectional area, and feed pressure known, calculation of flux and

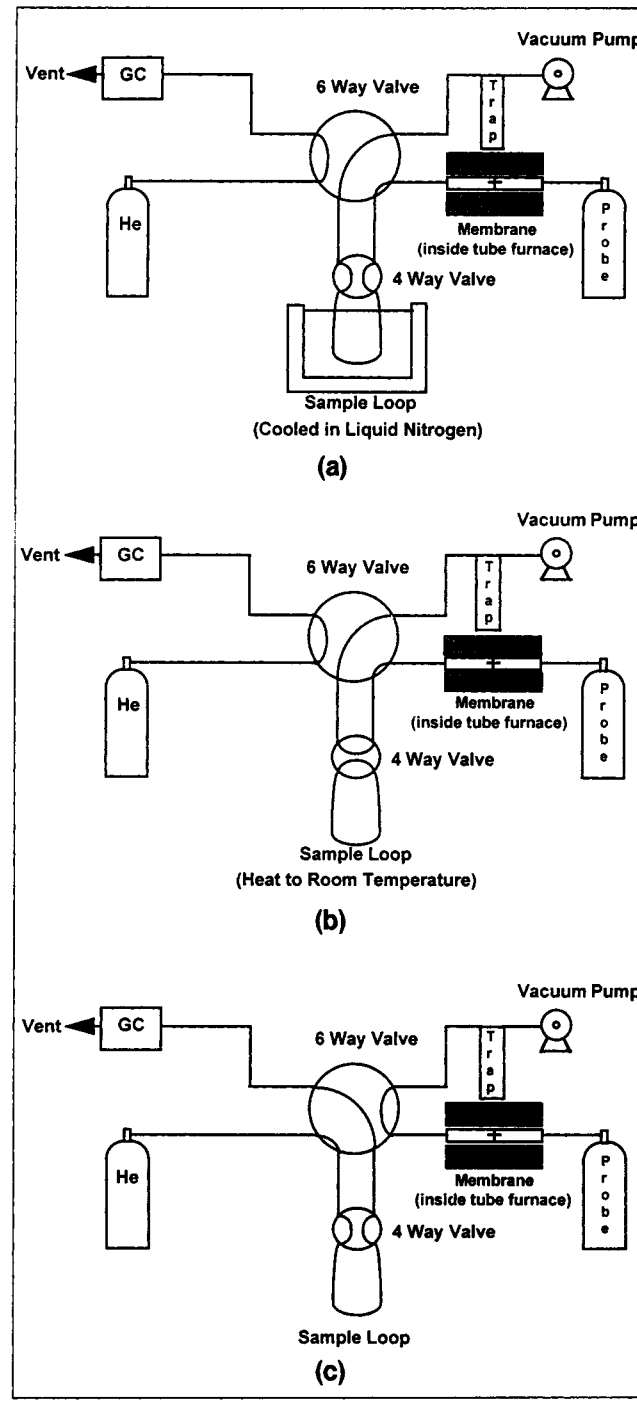

Figure 5. Permeation measurement apparatus and sampling procedure for measuring hydrocarbon flux: (a) collecting, (b) heating, (c) analyzing samples.

permeance was carried out. For all the measurements, partial pressure of the hydrocarbon at the permeate side could be neglected for the purpose of calculating the transmembrane pressure difference.

Results and Discussion

A series of physical adsorption experiments were con-

Table 2. Equilibrium Adsorption Capacity of Probe Molecules in Pure-Silica Ferrierite Crystals Ground to Micron Size

	Nitrogen	Methane	*n*-Butane	Isobutane
Equilibrium adsorption capacity [cm^3/g FER]	0.13	0.11	0.04	0.04
Isotherm temp. [K]	77	77	298	261
P_o [$\times 10^{-5}$ Pa]	1.01	0.02	2.69	1.00
Relative pres. (P/P_o)	0.4	0.4	0.4	0.6

ducted in order to assist in the selection of suitable probe molecules. The adsorption capacities listed in Table 2 are measured at temperatures (T) and pressures (P) chosen to allow for maximum possible saturation of the micropores in ferrierite and test size-exclusion of particular probe molecules based on uptakes. The void volumes calculated from the nitrogen and methane uptakes are 0.13 and 0.11 cm^3/g, respectively, which compare well with the void volume of 0.13 cm^3/g calculated from the crystal structure (Lewis et al., 1996). The void volume found by methane adsorption is slightly lower than the theoretical value and is likely due to incomplete filling of the micropores that results from the steric limitations in packing methane in the channels. Equilibrium adsorption uptakes for *n*-butane and isobutane indicate an adsorption capacity of 0.04 cm^3/g. Figure 1a shows that there are two 10-MR channels per unit cell (unit cells denoted by rectangular boxes). Assuming that the void space resulting from the 10-MR channels in one unit cell can be represented as two cylinders of diameter 5 Å and length 7.43 Å (*a*-axis length of ferrierite unit cell, Lewis et al., 1996), a volume of 0.04 cm^3/g is calculated. Thus, based on the adsorption data, nitrogen and methane molecules are able to access both the 8- and 10-MR-channel systems, while the *n*-butane and isobutane are only able to access the 10-MR-channel system (are size-excluded from the 8-MR-channel system). These results are consistent with the well-known molecular sieving effect by simple comparison of the adsorbate kinetic diameters and the 8- and 10-MR pore sizes.

In order to examine the degree of saturation of the zeolite by the probe molecules at the conditions of the permeation measurements, adsorption isotherms for *n*-butane and isobutane were measured at 383 K and are shown in Figure 6. At an absolute pressure of 1.01×10^5 Pa, the zeolite is saturated with *n*-butane, but contains very little isobutane. Thus, at the conditions used for the permeation experiments, the concentration of adsorbed *n*-butane is near saturation at the feed side and declines to zero toward the permeate side. However, the concentration of adsorbed isobutane remains low throughout the crystal.

Based on data from the adsorption experiments, a set of temperatures (323, 383 and 398 K) at a feed membrane pressure of 1.01×10^5 Pa were selected for permeation experiments. The upper temperature limit is set by the thermal stability of the epoxy used to seal the ferrierite crystals. Due to the thin line of epoxy used to construct the single-crystal membranes, leaks resulting from the thermal degradation of the epoxy occur after extended membrane operation at temperatures in excess of 403 K. The equilibrium hydrocarbon adsorption uptakes at the temperature and pressure selected

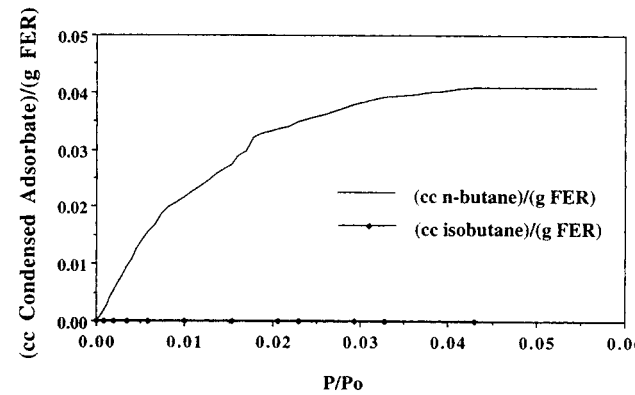

Figure 6. Adsorption isotherms of *n*-butane and isobutane collected at $T = 383$ K.

The final datum point on each of the isotherms represents a relative pressure corresponding to $P = 1.01 \times 10^5$ Pa.

for the permeation experiments are listed in Table 3. None of the methane and isobutane permeation experiments are conducted near adsorption-saturation conditions. In contrast, all of the *n*-butane permeation experiments are conducted at temperatures and feed pressure where the feed side of the crystals is saturated with *n*-butane.

The single-gas, steady-state permeation results for the single-crystal ferrierite membranes for different probe molecules as a function of crystal orientation and temperature are reported in Table 4. Several interesting trends are observed in these data. For methane transport in the 8-MR membrane configuration, the flux increases only slightly with temperature over the range of temperatures investigated. Based on the measured equilibrium adsorption capacity, methane is able to access both the 8- and 10-MR-ring channels. Therefore, in the 8-MR crystal-orientation experiments, methane can enter the 10-MR channels after entering the crystal since the two channel systems intersect. However, since there is no pressure gradient in the 10-MR direction, the 10-MR channels do not contribute to the measured fluxes. The relative pressures of methane for all the 8-MR/methane permeation experiments shown in Table 4 are sufficiently low so that the entire thickness of the membrane is far from saturation and most likely in the Henry's Law regime. No detectable *n*-butane or isobutane is observed through the 8-MR-oriented FER crystals, indicating that the *n*-butane and isobutane are

Table 3. Equilibrium Adsorption Uptakes Reported in [cm^3 Condensed Adsorbate/g FER] for Hydrocarbon Probe Molecules in Pure-Silica Ferrierite at 1.01×10^5 Pa Pressure and Three Temperatures Selected for Single-Crystal Membrane Permeation Experiments.*

Temperature	Methane	*n*-Butane	Isobutane
323 K	0.00 (0.003)	0.04 (0.20)	0.00 (0.16)
383 K	0.00 (0.002)	0.04 (0.059)	0.00 (0.044)
398 K	0.00 (0.002)	0.04 (0.05)	0.00 (0.04)

*Values listed in parentheses indicate relative pressure (P/P_o) at the feed side of single-crystal membrane.

Table 4. Single-Gas Steady-State Permeation through Single-Crystal Ferrierite Membranes at a Feed Pressure of 1.01×10^5 Pa as a Function of Crystal Orientation and Temperature

Crystal Orientation*	Temp. K	Probe Molecule	Permeance ($\times 10^{-12}$) mol/(m²·s·Pa)
8	323	methane	2.04
8	383	methane	2.12
8	398	methane	2.25
10	323	methane	41.1
10	383	methane	152
10	398	methane	186
10	323	*n*-butane	25.3
10	383	*n*-butane	105
10	398	*n*-butane	163
10	323	isobutane	0.83
10	383	isobutane	0.85
10	398	isobutane	1.07

*Average cross-sectional areas: 8 MR orientation = 9.63(7) $\times 10^{-9}$ m², 10 MR orientation = 1.18(9) $\times 10^{-8}$ m²; average number of pore openings: 8 MR orientation = 1.39(8) $\times 10^{10}$, 10 MR orientation = 8.95(2) $\times 10^9$; average diffusion path lengths: 8 MR orientation = 6.20(9) $\times 10^{-4}$ m, 10 MR orientation = 5.07(3) $\times 10^{-4}$ m.

size-excluded from the 8-MR membranes in agreement with the equilibrium adsorption capacities listed in Table 2. This result is also the hallmark signature of zeolite molecular sieving and confirms the absence of cracks and pinholes in the single-crystal or sealing epoxy.

A much higher methane flux is observed in the 10-MR-oriented crystals relative to the 8-MR flux at all selected temperatures, as would be expected from the larger free diameters of the 10-MR channels. The methane permeances through the 10-MR channels shows a sharp increase with temperature from 41.1×10^{-12} mol/(m²·s·Pa) at $T = 323$ K to 186×10^{-12} mol/(m²·s·Pa) at $T = 398$ K, both at feed pressure of 1.01×10^{-5} Pa. This strong temperature dependence is not observed for methane in the 8-MR channels where the permeance increased only slightly from 2.04×10^{-12} mol/(m²·s·Pa) to 2.25×10^{-12} mol/(m²·s·Pa) over the same temperature range. The differences in methane permeance between the 8- and 10-MR orientations originate from the smaller free diameter of the 8 MR (4.6 Å × 3.7 Å × 3.0 Å) vs. the 10 MR (5.4 Å × 5.4 Å × 4.2 Å).

All of the *n*-butane permeation experiments are conducted at temperatures and feed pressures capable of inducing near saturation of *n*-butane in a portion of the 10-MR channels. Similar to the methane in the 10-MR channels, the *n*-butane also exhibits a sharp increase in permeance with increasing temperature.

Table 4 shows the transport of isobutane through the 1-MR-oriented single-crystal membranes to be much slower than that of any of the other probe molecules for this crystal orientation. The reported isobutane kinetic diameter of 5.0 Å (Breck, 1974) is very close in size to the pore dimensions of 5.4 Å × 5.4 Å × 4.4 Å of the 10-MR channel (Lewis et al., 1996). Therefore, isobutane has low mobility and the approach to adsorption equilibrium requires several hours. In contrast, equilibrium uptake is reached within minutes for all other probe molecules. A similar trend is observed in the single-crystal permeation experiments. Steady-state permeation rates are obtained on a time scale of minutes for all gases except isobutane, which requires several hours. Changes in temperature over the range investigated produced only minor changes in the isobutane permeance.

Table 5. Mixed-Gas (45% *n*-Butane and 55% Isobutane) Steady-State Permeation Results for Single-Crystal Ferrierite Membranes

Crystal Orientation	Temp. K	Pressure Differential $\times 10^{-5}$ Pa	Probe Molecule	Permeance $\times 10^{-12}$ mol/(m²·s·Pa)	*n/i* Separation Factor
10	323	1.01	*n*-butane	23.5	59
			isobutane	0.40	
10	383	1.01	*n*-butane	98.2	116
			isobutane	0.85	

The results of the mixed-gas (45% *n*-butane and 55% isobutane) permeation experiments are reported in Table 5. In general, the mixed-gas permeances are lower than the single-gas permeances; however, high *n*-butane/isobutane selectivities are maintained. This is encouraging in that it demonstrates that high separation selectivities are possible even with mixed-gas feeds.

The high permeances and selectivities shown in Tables 4 and 5 are reproducible only when using fresh single-crystal membranes. For example, after measurement of isobutane permeance, a membrane becomes impermeable to other gases due to the plugging of the micropores by adsorbed isobutane that does not appear to completely desorb even after heating the crystal at 398 K under vacuum for one week. The epoxy component of the single-crystal membrane prevents reactivating the membrane at higher temperatures. The lack of *n*-butane transport on crystals that have preadsorbed isobutane contrasts the findings of selective transport of *n*-butane when the "fresh" membrane is contacted with the two gases simultaneously. This apparent anomaly can be explained by postulating the existence of a small fraction of sites where isobutane is strongly adsorbed and is desorbed extremely slowly so as to block the adsorption of other gases. When the two gases are simultaneously present from the beginning of the experiment, the *n*-butane adsorbs preferentially because of its higher mobility preventing the subsequent adsorption of isobutane.

Actually, it is not only preadsorbed isobutane that affects subsequent transport of other molecules. Preadsorption of methane that apparently desorbs rapidly and completely as detected by GC analysis caused marked reduction in the subsequent flux of other molecules. Such hysteresis phenomena are not surprising for the essentially 1-D channel system of ferrierite—the 8-MR channels are inaccessible to the butanes. In this 1-D pore system, transport takes place by single-file diffusion (Kärger and Ruthven, 1992; Tsikoyannis and Wei, 1990). The latter reference presents a penetrating analysis of diffusion in 1-D, 2-D, and 3-D pore networks, but application of their analysis to the present situation would require more extensive experimental results and considerable analytical effort that is beyond the scope of this work.

The objective of this work is to construct well-defined 8- and 10-MR single-crystal membranes with the intent of establishing experimental upper limits for separation factors obtainable in polycrystalline zeolite membranes of similar pore dimensions. To date, there has been one report of a

polycrystalline ferrierite membrane (Matsukata et al., 1994). Direct comparison of the single-crystal ferrierite data with the polycrystalline ferrierite data is not possible due to the different gases and temperatures used in the permeation experiments. However, data at comparable conditions for polycrystalline ZSM-5 membranes are available. The ZSM-5 structure is composed of intersecting 10-MR channels of slightly larger dimensions (5.3 Å × 5.6 Å and 5.1 Å × 5.5 Å) (Meier and Olson, 1992), so comparison to the 10-MR single-crystal results is possible. At $T = 381$ K, an *n*-butane/isobutane selectivity of 39.4 is reported from single-gas permeation measurements from a polycrystalline ZSM-5 membrane (Yan et al., 1996). This compares to a single-gas *n/i* selectivity of 123 from the single-crystal ferrierite membrane experiments conducted at $T = 383$ K and a membrane pressure differential of 1.01×10^5 Pa.

Conclusions

A technique for constructing leak-free, single-crystal ferrierite membranes is presented. By properly orienting the crystal in a membrane configuration, transport through either the 8- or 10-MR channel system may be studied. The 8-MR channels admit methane but not *n*-butane or isobutane, while the 10-MR channels admit methane, *n*-butane, and isobutane. Permeation experiments conducted with a mixed-gas feed (45% *n*-butane and 55% isobutane) show maintenance of high *n/i* selectivities comparable to the selectivities observed from the single-gas experiments. Additionally, the measured fluxes and separation factors are shown to depend on the exposure history of the crystal to different probe molecules.

Acknowledgments

Financial support for this work was provided by the National Science Foundation (grant no. CTS-9114829). The authors also wish to acknowledge helpful discussions with Yushan Yan.

Literature Cited

Breck, D. W., *Zeolite Molecular Sieves*, Krieger, Malabar, FL, p. 636 (1974).

Chen, N. Y., T. F. Degnan, Jr., and C. M. Smith, *Molecular Transport and Reaction in Zeolites*, VCH, New York, p. 131 (1994).

Dietz, W. A., "Response Factors for Gas Chromatographic Analyses," *J. Gas Chromatog.*, **5**, 68 (1967).

Gas Processors Suppliers Association (GPSA), *Engineering Data Book*, GPSA, Tulsa, OK, p. 23-1 (1987).

Gues, E. R., J. C. Jansen, and H. van Bekkum, "Calcination of Large MFI-Type Single Crystals: 1. Evidence for the Occurrence of Consecutive Growth Forms and Possible Diffusion Barriers Arising Thereof," *Zeolites*, **14**, 82 (1994).

Gues, E. R., and H. van Bekkum, "Calcination of Large MFI-Type Single Crystals: 2. Crack Formation and Thermomechanical Properties in View of the Preparation of Zeolite Membranes," *Zeolites*, **15**, 333 (1995).

Jansen, K. C., and E. N. Coker, "Zeolitic Membranes," *Curr. Opin. Solid State Mater. Sci.*, **1**, 65 (1996).

Kärger, J., and D. M. Ruthven, *Diffusion in Zeolites*, Wiley, New York, p. 207 (1992).

Kuperman, A., S. Nadimi, S. Oliver, G. A. Ozin, J. M. Garcés, and M. M. Olken, "Nonaqueous Synthesis of Giant Crystals of Zeolites and Molecular Sieves," *Nature*, **365**, 239 (1993).

Lewis, J. E., Jr., C. C. Freyhardt, and M. E. Davis, "Location of Pyridine Guest Molecules in an Electroneutral $\{^3_\infty\}[SiO_{4/2}]$ Host Framework: Single Crystal Structures of the As-synthesized and Calcined Forms of High-silica Ferrierite," *J. Phys. Chem.*, **100**, 5039 (1996).

Matsukata, M., N. Nishiyama, and K. Ueyama, "Preparation of a Thin Zeolitic Membrane," *Studies in Surface Science and Catalysis*, Vol. 84, J. Weitkamp, H. G. Karge, H. Pfeifer, and W. Hölderich, eds., Elsevier, Amsterdam, p. 1183 (1995).

Meier, W. M., and D. H. Olson, *Atlas of Zeolite Structure Types*, Butterworth-Heinemann, Boston, p. 138 (1992).

Nadimi, S., S. Oliver, A. Kuperman, A. Lough, G. A. Ozin, J. M. Garcés, M. M. Olken, and P. Rudolf, "Nonaqueous Synthesis of Large Zeolite and Molecular Sieve Crystals," *Proc. Int. Zeolite Conf.*, H. G. Karge, H. Pfeifer, and W. Hölderich, eds., Elsevier, Amsterdam, p. 93 (1995).

Paravar, A. R., and D. T. Hayhurst, "Direct Measurement of Diffusivity for Butane Across a Single Large Silicalite Crystal," *Proc. Int. Zeolite Conf.*, D. Olson and A. Bisio, eds., Butterworths, New York, p. 217 (1984).

Ruthven, D. M., "Diffusion in Zeolites," *Zeolites: A Refined Tool for Designing Catalytic Sites*, L. Bonneviot and S. Kaliaguine, eds., Elsevier, Amsterdam, p. 223 (1995).

Shah, D. B., S. Chokchalacha, and D. T. Hayhurst, "Measurements of Transport Rates of C_4 Hydrocarbons across a Single-Crystal Silicalite Membrane," *J. Chem. Soc. Farad. Trans.*, **89**(16), 3161 (1993).

Shah, D. B., and H. Y. Liou, "Diffusion of Aromatics Through a Silicalite Membrane," *Zeolites and Related Microporous Materials: State of the Art 1994*, Vol. 84, J. Weiktamp, H. G. Karge, H. Pfeifer, and W. Hölderich, eds., Elsevier, Amsterdam, p. 1347 (1994).

Tsikoyannis, J. G., and J. Wei, "Diffusion and Reaction in High-Occupancy Zeolite Catalysts—I. A Stochastic Theory," *Chem. Eng. Sci.*, **46**, 233 (1991).

van Koningsveld, H., J. C. Jensen, and H. van Bekkum, "The Monoclinic Framework Structure of Zeolite H-ZSM-5: Comparison with the Orthorhombic Framework of As-synthesized ZSM-5," *Zeolites*, **10**, 235 (1990).

Weast, R. C., M. J. Astle, and W. H. Beyer, eds., *CRC Handbook of Chemistry and Physics*, CRC, Boca Raton, FL (1986).

Weigel, S. J., J. C. Gabriel, E. G. Puebla, A. M. Bravo, N. J. Henson, L. M. Bull, and A. K. Cheetham, "Structure-Directing Effects in Zeolite Synthesis—A Single-Crystal X-Ray Diffraction, ^{29}Si MAS NMR, and Computational Study of the Competitive Formation of Siliceous Ferrierite and Dodecasil-3C (ZSM-39)," *J. Amer. Chem. Soc.*, **118**(10), 2427 (1996).

Wernick, D. L., and E. J. Osterhuber, "Diffusional Transition in Zeolite NaX: 1. Single Crystal Gas Permeation Studies," *Proc. Int. Zeolite Conf.*, D. Olson and A. Bislo, eds., Butterworths, New York, p. 22 (1984).

Yan, Y., M. E. Davis, and G. R. Gavalas, "Preparation of Highly Selective Zeolite ZSM-5 Membranes by a Post-synthetic Coking Treatment," *J. Memb. Sci.*, in press.

Manuscript received Apr. 24, 1996, and revision received July 12, 1996.